Thermodynamic theory of epitaxial ferroelectric thin films with dense domain structures

V. G. Koukhar,[1] N. A. Pertsev,[1,2,*] and R. Waser[2,3]

[1]A. F. Ioffe Physico-Technical Institute, Russian Academy of Sciences, 194021 St. Petersburg, Russia
[2]Institut für Werkstoffe der Elektrotechnik, RWTH Aachen University of Technology, D-52056 Aachen, Germany
[3]Elektrokeramische Materialen, Institut für Festkörperforschung, Forschungszentrum Jülich, D-52425 Jülich, Germany

A Landau-Ginsburg-Devonshire-type nonlinear phenomenological theory is presented, which enables the thermodynamic description of dense laminar polydomain states in epitaxial ferroelectric thin films. The theory explicitly takes into account the mechanical substrate effect on the polarizations and lattice strains in dissimilar elastic domains (twins). Numerical calculations are performed for $PbTiO_3$ and $BaTiO_3$ films grown on (001)-oriented cubic substrates. The ''misfit strain-temperature'' phase diagrams are developed for these films, showing stability ranges of various possible polydomain and single-domain states. Three types of polarization instabilities are revealed for polydomain epitaxial ferroelectric films, which may lead to the formation of new polydomain states forbidden in bulk crystals. The total dielectric and piezoelectric small-signal responses of polydomain films are calculated, resulting from both the volume and domain-wall contributions. For $BaTiO_3$ films, strong dielectric anomalies are predicted at room temperature near special values of the misfit strain.

I. INTRODUCTION

In thin films of perovskite ferroelectrics epitaxially grown on many substrates, the lattice misfit of the epitaxial couple creates a driving force for the formation of regular ferroelastic domain (twin) structures below the phase transition temperature. The twinning of epitaxial layers was predicted theoretically by Roitburd already in 1976,[1] and during the past decade domain patterns were found in $PbTiO_3$, $Pb(Zr_xTi_{1-x})O_3$, $(Pb_{1-x}La_x)TiO_3$, $BaTiO_3$, $KNbO_3$, and $SrBi_2Ta_2O_9$ films grown on various single-crystalline substrates.[2–20]

The experimental observations triggered intensive theoretical studies of the statics and dynamics of elastic domains (twins) in epitaxial ferroelectric and ferroelastic thin films.[21–37] In the general case, the problem is very complicated because of substantial inhomogeneity of internal mechanical stresses in polydomain (twinned) films. For a domain configuration with an arbitrary geometry, the solution may be found with the aid of the dislocation-disclination modeling of the stress sources existing in epitaxial layers at the film/substrate interface and junctions of ferroelastic domain walls.[25,26,30,37] The complexity of this theoretical approach, however, reduces to a reasonable level only in a linear elastic approximation, which neglects deviations of the order parameters in thin films from their equilibrium values in stress-free bulk crystals. In the case of ferroelectric films, on the contrary, the mechanical substrate effect may strongly change the polarization components, as shown recently for single-domain films with the aid of a nonlinear thermodynamic theory.[38,39] Therefore, a rigorous theoretical analysis, which does not employ the linear approximation, is required to describe polydomain states in epitaxial ferroelectric films correctly.

The basis for this analysis is provided by the Landau-Ginsburg-Devonshire phenomenological theory, which was widely used in the past to explain physical properties of bulk ferroelectrics.[40–42] To make the nonlinear description of polydomain films mathematically feasible, it is necessary to assume the polarization and strain fields to be homogeneous within each domain. This approximation may be justified for dense laminar polydomain states, where the domain widths are much smaller than the film thickness.[36] Such domain structures become energetically most favorable in epitaxial films with a thickness larger than about 100 nm.[26]

In this paper, a nonlinear Landau-Ginsburg-Devonshire-type thermodynamic theory is developed for polydomain epitaxial films of perovskite ferroelectrics. The method of theoretical calculations is reported, which makes it possible to determine polarizations, lattice strains, and mechanical stresses inside dissimilar domains forming dense laminar structures (Sec. II). For $PbTiO_3$ and $BaTiO_3$ films grown on dissimilar cubic substrates, the ''misfit strain-temperature'' phase diagrams are constructed, which show the stability ranges of various possible polydomain and single-domain states (Sec. III). The small-signal dielectric responses of polydomain $PbTiO_3$ and $BaTiO_3$ epitaxial films are calculated numerically, and their changes at the misfit-strain-driven structural transformations are discussed (Sec. IV). The piezoelectric properties of polydomain ferroelectric thin films are also determined (Sec. V). Finally, some general features of the polydomain (twinned) states in epitaxial ferroelectric films are discussed, and the theoretical predictions are compared with available experimental data (Sec. VI).

It should be emphasized that the developed nonlinear theory enables the calculation of the total dielectric and piezoelectric responses of polydomain thin films with the account of the mechanical substrate effect. This feature of the theory demonstrates its great practical importance, because ferroelectric thin films have many possible applications in advanced microelectronic and micromechanical devices.[43,44]

II. METHOD OF THEORETICAL CALCULATIONS

We will discuss single-crystalline epitaxial films grown in a paraelectric state on much thicker dissimilar substrates. During the cooling from the deposition temperature T_g, the paraelectric-to-ferroelectric phase transition is assumed to take place in the film. This transition leads to the formation of either a single-domain or a polydomain state. In the simplest case, the latter is composed of alternating domains of two types. According to the observations, the ferroelastic domain structure of an epitaxial film may be modeled by a periodic array of parallel planar walls. The geometry of this laminar pattern is defined by the domain-wall periodicity D and the volume fraction ϕ of domains of the first type in the film.

In relatively thick films the domain widths are expected to be much smaller than the film thickness H.[23,26] In this case of a dense structure ($D \ll H$), the polarization and strain fields become almost uniform within each domain in the inner region of the film, because highly inhomogeneous internal fields can exist only in two thin layers ($h \sim D$) near the film surfaces[1] [see Fig. 1(a)]. Therefore, the distribution of the energy density in a polydomain film may be regarded as *piecewise homogeneous* when calculating the total free energy $\mathcal{F}$ of the epitaxial system. Indeed, the contribution of the inner region to the energy $\mathcal{F}$ is about H/D times larger than the contribution of the surface layers, so that the latter may be neglected at $D \ll H$ in the first approximation. The elastic energy stored in a substrate having elastic compliances similar to those of the film can be ignored on the same grounds. The contribution of the self-energies of domain walls also can be neglected in the range of film thicknesses $H \gg 100 H_0$, where the condition $D \ll H$ becomes valid.[26] This contribution scales as $\sqrt{H}$ here because it is proportional to H/D and the equilibrium domain period $D \sim \sqrt{H}$.[26] Accordingly, the film elastic strain energy is $\sqrt{H/H_0}$ times larger than the overall self-energy of domain walls, where $H_0 \sim 1$ nm is the characteristic film thickness described in Ref. 26.

In the resulting approximation, equilibrium values of polarization components $P_i (i = 1,2,3)$ and lattice strains S_n ($n = 1,2,3, \ldots , 6$ in the Voigt matrix notation) inside domains of two types and their equilibrium volume fractions become independent of the domain period D and film thickness H. The calculation of these parameters defining piecewise homogeneous fields in the inner region of a polydomain film represents the goal of the present theory. Determination of the equilibrium domain period D^* remains beyond the scope of this theory because D^* is governed by the competition of the overall self-energy of domain walls and the energy stored in the surface layers. However, the equilibrium period D^* may be evaluated in the linear elastic approximation. The calculations show[26] that the inequality $D^* \ll H$ indeed holds for sufficiently thick films ($H \gg 100$ nm in the case of PbTiO$_3$ and BaTiO$_3$ films).

For the correct thermodynamic description of polydomain thin films, an appropriate form of the free-energy function must be chosen, which corresponds to the actual boundary conditions of the problem. In this paper, we shall assume that
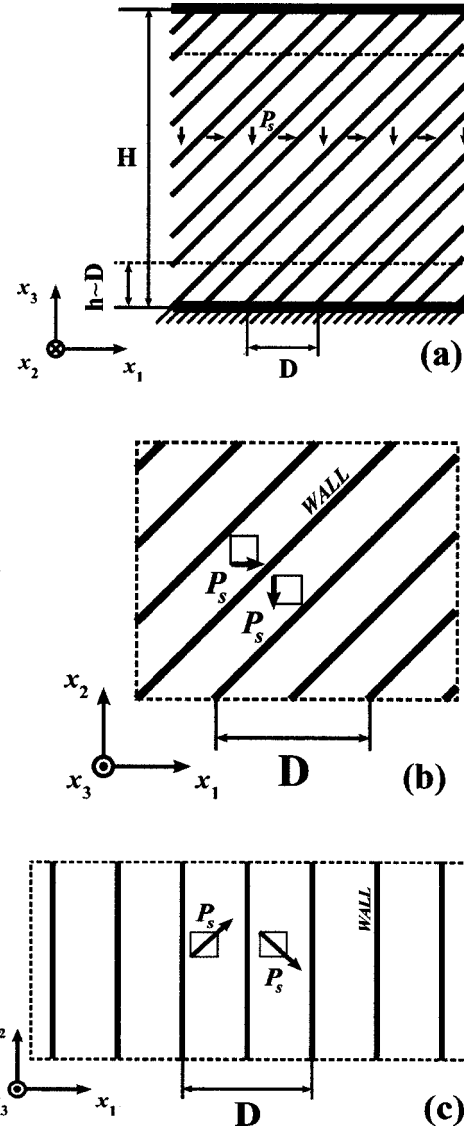

FIG. 1. Schematic drawing of the dense $c/a/c/a$ (a), $a_1/a_2/a_1/a_2$ (b), and $aa_1/aa_2/aa_1/aa_2$ (c) domain structures in epitaxial thin films of perovskite ferroelectrics. H is the film thickness; $D \ll H$ is the domain-wall periodicity. The dashed line indicates a thin layer near the film/ substrate interface, where internal stresses are highly inhomogeneous. The x_3 axis of the rectangular reference frame (x_1, x_2, x_3) is orthogonal to the interface, whereas the x_1 and x_2 axes are parallel to the in-plane crystallographic axes of the film prototypic cubic phase.

the film is kept under an external electric field $\mathbf{E}_0$, but the film/substrate system is not subjected to external mechanical forces. Since there is no work done by such forces, the free energy $\mathcal{F}$ of the heterostructure can be derived solely from the spatial distribution of the Helmholtz free-energy density.

We focus now on (001)-oriented perovskite films epitaxially grown on a cubic substrate with the surface parallel to the (001) crystallographic planes. For bulk perovskite ferroelectrics, thermodynamic calculations usually employ the Gibbs energy function G.[41,42] It may be approximated by a six-degree polynomial in polarization components P_i:

$$G = \alpha_1(P_1^2 + P_2^2 + P_3^2) + \alpha_{11}(P_1^4 + P_2^4 + P_3^4) + \alpha_{12}(P_1^2 P_2^2 + P_1^2 P_3^2 + P_2^2 P_3^2) + \alpha_{111}(P_1^6 + P_2^6 + P_3^6) + \alpha_{112}[P_1^4(P_2^2 + P_3^2)$$

$$+ P_3^4(P_1^2 + P_2^2) + P_2^4(P_1^2 + P_3^2)] + \alpha_{123}P_1^2 P_2^2 P_3^2 - \frac{1}{2}s_{11}(\sigma_1^2 + \sigma_2^2 + \sigma_3^2) - s_{12}(\sigma_1\sigma_2 + \sigma_1\sigma_3 + \sigma_3\sigma_2) - \frac{1}{2}s_{44}(\sigma_4^2 + \sigma_5^2 + \sigma_6^2)$$

$$- Q_{11}(\sigma_1 P_1^2 + \sigma_2 P_2^2 + \sigma_3 P_3^2) - Q_{12}[\sigma_1(P_2^2 + P_3^2) + \sigma_3(P_1^2 + P_2^2) + \sigma_2(P_1^2 + P_3^2)] - Q_{44}(P_2 P_3 \sigma_4 + P_1 P_3 \sigma_5 + P_2 P_1 \sigma_6),$$

$$\tag{1}$$

where σ_n are the internal mechanical stresses in the film, α_1, α_{ij}, and α_{ijk} are the dielectric stiffness and higher-order stiffness coefficients at constant stress,[41,42] S_{mn} are the elastic compliances at constant polarization, and Q_{ij} are the electrostrictive constants of the paraelectric phase. Since the standard Gibbs function (1) is not appropriate for the description of thin films,[38] a modified thermodynamic potential or the Helmholtz free-energy function F should be used in this case.[38,39] The latter can be derived via the inverse Legendre transformation of G, which gives $F = G + \Sigma_{n=1}^{6}\sigma_n S_n$. Substituting Eq. (1) into this formula and eliminating the strains with the aid of thermodynamic relations $S_n = -\partial G/\partial\sigma_n$,[42] after some manipulation we obtain the energy density F as a function of P_i and σ_n. For the relevant modified density $\tilde{F}$,[45] which allows for the possible presence of the *internal* electric field $\mathbf{E}$ in a film and for the fact that the electrostatic potentials of electrodes are fixed in our case but not their charges, the calculation gives (ε_0 is the permittivity of the vacuum)

$$\tilde{F} = \alpha_1(P_1^2 + P_2^2 + P_3^2) + \alpha_{11}(P_1^4 + P_2^4 + P_3^4)$$
$$+ \alpha_{12}(P_1^2 P_2^2 + P_1^2 P_3^2 + P_2^2 P_3^2) + \alpha_{111}(P_1^6 + P_2^6 + P_3^6)$$
$$+ \alpha_{112}[P_1^4(P_2^2 + P_3^2) + P_2^4(P_1^2 + P_3^2) + P_3^4(P_1^2 + P_2^2)]$$
$$+ \alpha_{123}P_1^2 P_2^2 P_3^2 + \frac{1}{2}s_{11}(\sigma_1^2 + \sigma_2^2 + \sigma_3^2)$$
$$+ s_{12}(\sigma_1\sigma_2 + \sigma_1\sigma_3 + \sigma_2\sigma_3) + \frac{1}{2}s_{44}(\sigma_4^2 + \sigma_5^2 + \sigma_6^2)$$
$$- \frac{1}{2}\varepsilon_0(E_1^2 + E_2^2 + E_3^2) - E_1 P_1 - E_2 P_2 - E_3 P_3. \tag{2}$$

It should be noted that Eq. (2) is written in the crystallographic frame (x_1, x_2, x_3) of the paraelectric phase, and we shall take the x_3 axis to be orthogonal to the substrate (Fig. 1). The dielectric stiffness α_1 will be given a linear temperature dependence $\alpha_1 = (T - \theta)/2\varepsilon_0 C$ based on the Curie-Weiss law (θ and C are the Curie-Weiss temperature and constant). We also emphasize that, despite the formal absence of the electrostrictive terms in Eq. (2), $\tilde{F}$ still takes into account the coupling between the polarization and strain in full measure. Indeed, the transformation of $\tilde{F}$ into a function of P_i and S_n restores the coupling terms.

Since we are considering here only periodic domain structures, the minimization of the total free energy $\mathcal{F}$ may be replaced by the minimization of the energy density $\langle\tilde{F}\rangle$ averaged over the domain period D and the film thickness H. For dense structures, the mean density $\langle\tilde{F}\rangle$ can be evaluated from the relation $\langle\tilde{F}\rangle = \phi\tilde{F}' + (1 - \phi)\tilde{F}''$, where $\tilde{F}'$ and $\tilde{F}''$ are the characteristic energy densities in the inner regions of domains of the first and second type, within which the polarization and strain fields are almost uniform.

Using the mechanical and electric boundary conditions, it is possible to eliminate the stresses σ_i', σ_i'' and internal electric fields E_i', E_i'' from the final expression for the mean energy density $\langle\tilde{F}\rangle$, which follows from Eq. (2). Since changes of the in-plane sizes and shape of the film during its cooling from the deposition temperature are controlled by a much thicker substrate, the mean in-plane strains $\langle S_1\rangle$, $\langle S_2\rangle$, and $\langle S_6\rangle$ must be fixed quantities at a given temperature. For films grown on (001)-oriented cubic substrates, this condition gives

$$\phi S_1' + (1 - \phi)S_1'' = S_m, \quad \phi S_2' + (1 - \phi)S_2'' = S_m,$$

$$\phi S_6' + (1 - \phi)S_6'' = 0, \tag{3}$$

where $S_m = (b^* - a_0)/b^*$ is the misfit strain[38,39] in the heterostructure (b^* is the substrate effective lattice parameter,[24] and a_0 is the equivalent cubic cell constant of the free-standing film). Using Eqs. (3) together with the relations $S_n = -\partial G/\partial\sigma_n$, we obtain the first three conditions imposed on the stresses σ_i', σ_i'' inside domains of two types. Another three conditions follow from the absence of tractions on the free surface of the film. The mean values of the stress components σ_3, σ_4, and σ_5, therefore, must be zero in the film.

The local electric fields $\mathbf{E}'$ and $\mathbf{E}''$ in a polydomain ferroelectric film are not necessarily equal to the external field $\mathbf{E}_0$ defined by the potential difference between the electrodes. This effect may be caused by the presence of polarization charges at the film surfaces and even on domain boundaries. (We do not consider here films with other sources of internal fields, like charged vacancies, point defects, and depletion layers.[46]) The surface depolarization field, however, may be ignored in relatively thick ($H > 100$ nm) films of perovskite ferroelectrics, which are discussed in this paper. Indeed, the calculations taking into account the actual finite conductivity of these ferroelectrics show that the film depolarizing field is negligible.[47] Therefore, the mean electric field $\langle\mathbf{E}\rangle$ in the film may be set equal to the applied field $\mathbf{E}_0$.

In addition to the above nine macroscopic conditions, we can introduce ''microscopic'' boundary conditions on the do-

main walls. Indeed, the fields existing in adjacent domains are interrelated in the following way. First, the lattice strains in the polydomain layer must obey the classical compatibility condition.[48] In the rotated coordinate system (x_1', x_2', x_3') with the x_3' axis orthogonal to the walls, this requirement gives $S_1' = S_1''$, $S_2' = S_2''$, and $S_6' = S_6''$. Second, from the equations of mechanical equilibrium[49] it follows that in the absence of body forces $\sigma_3' = \sigma_3''$, $\sigma_4' = \sigma_4''$, and $\sigma_5' = \sigma_5''$. Third, the electric continuity conditions yield $E_1' = E_1''$, $E_2' = E_2''$, and $\varepsilon_0 E_3' + P_3' = \varepsilon_0 E_3'' + P_3''$.

The resulting 18 relationships make it possible to express internal stresses σ_i', σ_i'' and electric fields E_i', E_i'' inside domains of two types in terms of polarization components P_i', P_i'' and the relative domain population ϕ. After the substitution of these expressions into Eq. (2), the average energy density $\langle \widetilde{F} \rangle$ becomes a function of seven variables: P_i', P_i'' ($i = 1,2,3$), and ϕ. Performing numerically the minimization of $\langle \widetilde{F} \rangle (P_i', P_i'', \phi)$, we can find the equilibrium polarizations in both domains and the equilibrium domain population ϕ^*. As follows from Eqs. (2) and (3), these parameters depend on the misfit strain S_m, temperature T, and the applied electric field $\mathbf{E}_0$. The minimum energy $\langle \widetilde{F} \rangle^* (S_m, T, \mathbf{E}_0)$ of the polydomain state can be also determined as a function of S_m, T, and $\mathbf{E}_0$.

On the basis of these calculations, the complete thermodynamic description of dense polydomain states in single-crystalline films may be developed. This is a complicated task because several domain configurations, which differ by the spatial orientation of domain walls, are possible in epitaxial films. The theoretical analysis must include the comparison of the energies $\langle \widetilde{F} \rangle^*$ of different polydomain states with each other and with the energies of single-domain states, which can be also calculated with the aid of our theory. On this basis, the stability ranges of various thermodynamic states in the misfit strain-temperature plane may be determined for short-circuited films ($\mathbf{E}_0 = 0$). Using the constructed (S_m, T) phase diagrams, the small-signal dielectric and piezoelectric constants of ferroelectric films may be computed as functions of the misfit strain and temperature. Moreover, the electric-field dependence of the film average polarization and its material constants can be studied, as well as the field-induced structural transformations in an epitaxial layer.

III. PHASE DIAGRAMS OF PbTiO₃ AND BaTiO₃ EPITAXIAL THIN FILMS

For PbTiO₃ (PT) and BaTiO₃ (BT) films, quantitative results may be obtained with the aid of the procedure described in Sec. II, because the material parameters involved in the thermodynamic calculations are known for PT and BT to a good degree of precision. Using the values[50] of these parameters taken from Refs. 40–42, we have performed necessary numerical calculations and developed the misfit strain-temperature phase diagrams of short-circuited ($\mathbf{E}_0 = 0$)PT and BT films, which will be described in this section.

The following three variants of the orientation of domain walls were assumed to be possible in epitaxial films of perovskite ferroelectrics grown on cubic substrates.

(i) Domain walls are parallel to the {101} crystallographic planes of the prototypic cubic phase so that they are inclined at about 45° to the film/substrate interface Σ. This variant of domain geometry corresponds to the so-called $c/a/c/a$ structure widely observed in epitaxial films of perovskite ferroelectrics [Fig. 1(a)].[2,6,10,11] It is composed of alternating pseudotetragonal c domains and pseudotetragonal a domains, where the spontaneous polarization $\mathbf{P}_s$ is orthogonal to the interface Σ in the c domains and parallel to Σ in the a domains, being directed along the [100] axis of the prototypic phase in the latter.

(ii) Domain walls are orthogonal to the film/substrate interface and oriented along the {110} planes of the prototypic cubic phase. This domain-wall orientation is characteristic of the so-called $a_1/a_2/a_1/a_2$ structure, where the spontaneous polarization $\mathbf{P}_s$ develops in the film plane along the [100] and [010] axes within the a_1 and a_2 domains, respectively [Fig. 1(b)]. Domain walls with this orientation were observed experimentally in PbTiO₃ epitaxial films.[6,8]

(iii) The walls are taken to be parallel to the {100} or {010} planes of the prototypic lattice, as expected for the domain patterning in the orthorhombic aa phase, which was predicted to form in single-domain PT and BT films at positive misfit strains.[38] The corresponding polydomain state may consist of orthorhombic aa_1 and aa_2 domains with $\mathbf{P}_s$ directed along the [110] and [1$\bar{1}$0] axes of the cubic lattice, respectively [see Fig. 1(c)]. In this $aa_1/aa_2/aa_1/aa_2$ structure, domain walls are also perpendicular to the substrate surface, but their orientation in the film plane differs from the preceding variant by 45°.

For each of the above three orientations of domain walls, the energetically most favorable polarization configurations at various temperatures T and misfit strains S_m were determined, and the minimum energies $\langle \widetilde{F} \rangle^* (S_m, T, \mathbf{E}_0 = 0)$ of corresponding polydomain states were evaluated and compared. The comparison was also made with the energy of the paraelectric phase ($P_1 = P_2 = P_3 = 0$) and with the minimum energies of homogeneous ferroelectric states possible in PT and BT epitaxial films, i.e., the c phase ($P_1 = P_2 = 0$, $P_3 \neq 0$), the ca phase ($P_1 \neq 0$, $P_2 = 0$, $P_3 \neq 0$), the aa phase ($P_1 = P_2 \neq 0$, $P_3 = 0$), and the r phase ($P_1 = P_2 \neq 0$, $P_3 \neq 0$).[38] Selecting then the energetically most favorable thermodynamic state for each point of the misfit strain-temperature plane, we obtained the equilibrium phase diagrams of PT and BT epitaxial films shown in Fig. 2.

It should be emphasized that these diagrams differ considerably from those reported in our preceding paper.[36] The diagrams developed in Ref. 36 have a different meaning and may be considered as preliminary diagrams of PT and BT films. They describe the competition between the formation of single-domain states and the appearance of the polydomain $c/a/c/a$ one, as well as the transformations of the latter into heterophase states in those situations, where the orientation of internal boundaries along the {101} crystallographic planes is frozen in. Therefore, the diagrams given in Ref. 36 provide an important information as well. Indeed, they pre-
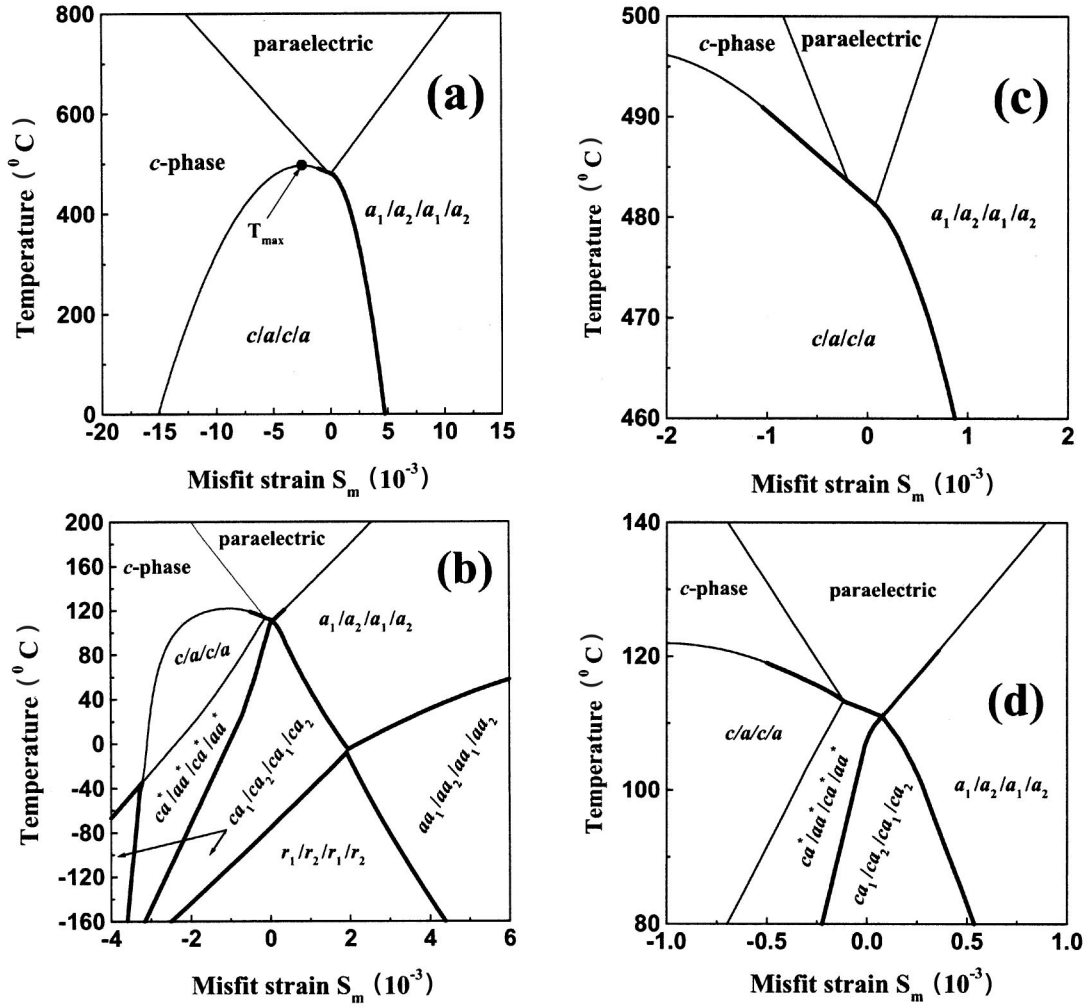
FIG. 2. Phase diagrams of PbTiO$_3$ (a), (c) and BaTiO$_3$ (b), (d) epitaxial films grown on cubic substrates. The continuous and discontinuous transformations are shown by thin and thick lines, respectively. Enlarged sections of the diagrams near $S_m=0$ are shown in (c) and (d).

dict *metastable states*, which may appear under experimental conditions, where the formation of alternative polydomain states (with walls orthogonal to the substrate surface) is impossible due to kinetic reasons.

Let us discuss the equilibrium diagrams shown in Fig. 2 in detail, focusing first on the diagram of PbTiO$_3$ films. At negative misfit strains S_m, except for a narrow strain range in the vicinity of $S_m=0$, the paraelectric-to-ferroelectric transformation results in the appearance of the tetragonal c phase with the spontaneous polarization $\mathbf{P}_s$ orthogonal to the substrate. This result agrees with the earlier prediction.[36] Compressive in-plane stresses σ_1 and σ_2 in the ferroelectric phase prevent the film from twinning at negative misfit strains S_m and relatively high temperatures T. During the further cooling of the epitaxial system, however, the introduction of elastic a domains into the c phase becomes energetically favorable. This leads to the formation of the pseudotetragonal $c/a/c/a$ polydomain state with the standard "head-to-tail" polarization configuration and 90° walls [Fig. 3(a)].

The calculation shows that the spontaneous polarization

$\mathbf{P}_s$ has the same magnitude in the c and a domains and varies with the misfit strain and temperature according to the relation

$$P_s^2 = -\frac{\alpha_{33}^{**}}{3\alpha_{111}} + \left(\frac{\alpha_{33}^{**2}}{9\alpha_{111}^2} - \frac{\alpha_3^{**}}{3\alpha_{111}}\right)^{1/2}, \qquad (4)$$

where $\alpha_3^{**} = \alpha_1 - (Q_{12}/s_{11})S_m$ and $\alpha_{33}^{**} = \alpha_{11} + Q_{12}^2/2s_{11}$ are the renormalized coefficients of the second-order polarization term P_3^2 and the fourth-order term P_3^4 in the free-energy expansion (2). Internal electric fields and the stresses σ_3, σ_4, σ_5, and σ_6 are absent in the $c/a/c/a$ structure. The equilibrium fraction of c domains equals

$$\phi_c^* = 1 - \frac{(s_{11}-s_{12})(S_m - Q_{12}P_s^2)}{s_{11}(Q_{11}-Q_{12})P_s^2}, \qquad (5)$$

and, at $\phi_c = \phi_c^*$, the stresses σ_1^a and σ_1^c also vanish, whereas the stress σ_2 acquires the same value of $\sigma_2^a = \sigma_2^c = (S_m$
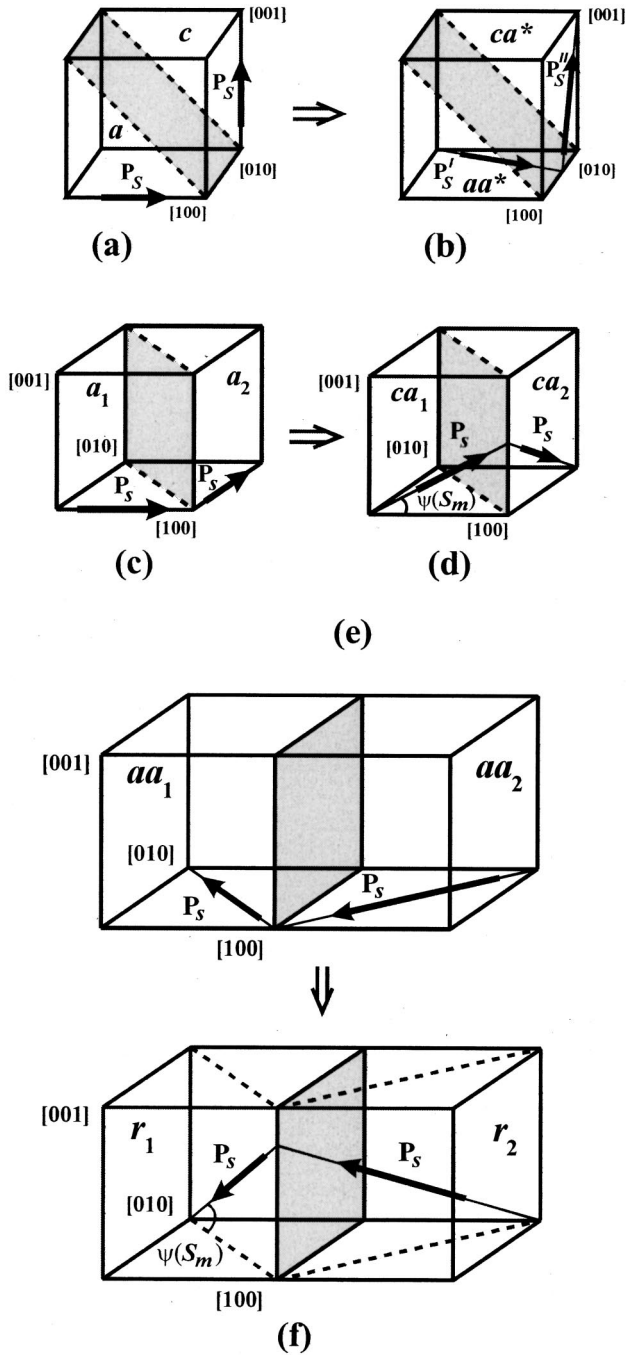
FIG. 3. Polarization patterning in various polydomain states forming in ferroelectric films: $c/a/c/a$ (a), $ca^*/aa^*/ca^*/aa^*$ (b), $a_1/a_2/a_1/a_2$ (c), $ca_1/ca_2/ca_1/ca_2$ (d), $aa_1/aa_2/aa_1/aa_2$ (e), and $r_1/r_2/r_1/r_2$ (f). Polarization orientations are shown relative to the prototypic cubic cell.

$-Q_{12}P_s^2)/s_{11}$ in both domains. The free-energy density $\langle \tilde{F} \rangle^*(S_m, T, \mathbf{E}_0 = 0)$ in the equilibrium $c/a/c/a$ polydomain state may be written as

$$\langle \tilde{F} \rangle^* = \frac{S_m^2}{2s_{11}} + \alpha_3^{**} P_s^2 + \alpha_{33}^{**} P_s^4 + \alpha_{111} P_s^6, \quad (6)$$

with P_s^2 given by Eq. (4).

Consider now the stability range R_d of the $c/a/c/a$ domain pattern in the (S_m, T) phase diagram. The boundary of R_d, which is shown by a thin line in Fig. 2(a), is defined by the inequality $\phi_c^*(S_m) < 1$ imposed on the equilibrium volume fraction of c domains. From Eq. (5) it follows that ϕ_c^* becomes equal to unity at $S_m^0(T) = Q_{12}P_0^2(T)$, where P_0 is the spontaneous polarization of a mechanically free crystal. The line $S_m^0(T) = Q_{12}[-\alpha_{11} + \sqrt{\alpha_{11}^2 - 3\alpha_1(T)\alpha_{111}}]/3\alpha_{111}$ constitutes the left-hand boundary of R_d, which is limited by the upper point of R_d located at temperature $T_{max} = \theta + 2\varepsilon_0 C\alpha_{11}^2/3\alpha_{111} \approx 497\,°C$ and misfit strain $S_m^0(T_{max}) = Q_{12}(-\alpha_{11}/3\alpha_{111}) \approx -2.4 \times 10^{-3}$ [see Fig. 2(a)]. The high-temperature section of the right-hand boundary, which adjoins this upper point, is defined by the curve $S_m^0(T) = Q_{12}[-\alpha_{11} - \sqrt{\alpha_{11}^2 - 3\alpha_1(T)\alpha_{111}}]/3\alpha_{111}$. This part of $S_m^0(T)$ relates to the second possible solution for P_0^2 that exists at $T > \theta$ in crystals with $\alpha_{11} < 0$ and $\alpha_{111} > 0$.

The next section of the right-hand boundary of R_d is formed by a short segment of the straight line, above which the solution (4) for the polarization in the $c/a/c/a$ state loses its physical meaning (here $\alpha_{33}^{**2} < 3\alpha_3^{**}\alpha_{111}$). At the part of this segment situated between two triple points [see Fig. 2(c)], the direct transformation of the paraelectric phase into the polydomain $c/a/c/a$ state takes place at the temperature

$$T_{c/a}(S_m) = \theta + \frac{2}{3}\varepsilon_0 C \frac{\alpha_{33}^{**2}}{\alpha_{111}} + 2\varepsilon_0 C \frac{Q_{12}}{s_{11}} S_m. \quad (7)$$

The ferroelectric phase transition in this "misfit-strain window" near $S_m = 0$ is of the *first order*, in contrast to the rest of the upper transition line, where it is of the *second order*. This is due to the fact that in PT (and also in BT) the renormalized coefficient α_{33}^{**} is *negative*. The result obtained here corrects the earlier prediction[38] that in epitaxial PT and BT films the ferroelectric phase transition is expected to be always of second order.

The remaining part of the right-hand boundary of R_d, also shown by a thick line in Fig. 2(a), separates the stability ranges of the $c/a/c/a$ and $a_1/a_2/a_1/a_2$ domain patterns in the (S_m, T) plane. At larger positive misfit strains, the $a_1/a_2/a_1/a_2$ polarization configuration becomes the most energetically favorable thermodynamic state in PT films. The instability of the $c/a/c/a$ pattern with respect to the appearance of the polarization component P_2 parallel to the domain walls, which was described in Ref. 36, does not manifest itself in the diagram of *equilibrium states*. This P_2 instability occurs in PT films at positive misfit strains $S_m^*(T)$ outside R_d. However, the P_2 instability may be revealed by preparing a film with the equilibrium $c/a/c/a$ structure first and then bending the substrate to increase S_m above $S_m^*(T)$ at a low temperature, where the formation of the $a_1/a_2/a_1/a_2$ state is suppressed.[36]

In the $a_1/a_2/a_1/a_2$ domain structure, the geometry of polarization patterning corresponds to the "head-to-tail" polarization configuration observed in bulk perovskite crystals.[40] The spontaneous polarization $\mathbf{P}_s$ has the same magnitude in the a_1 and a_2 domains and lies along the edges of the prototypic cubic cell, which are parallel to the film

surfaces [see Fig. 3(c)]. The equilibrium volume fractions of the a_1 and a_2 domains were found to be equal to each other at all investigated misfit strains and temperatures (ϕ^* =0.5), which agrees with the result obtained earlier in the linear elastic approximation.[23,26,29] Internal electric fields and the stress components σ_3, σ_4, σ_5, and σ_6 are absent in the $a_1/a_2/a_1/a_2$ structure. The stresses σ_1 and σ_2 are homogeneous inside the film and, at the equilibrium domain population of $\phi^*=0.5$, acquire the same value of $\sigma_1=\sigma_2=[S_m -0.5(Q_{11}+Q_{12})P_s^2]/(s_{11}+s_{12})$. In the rotated coordinate system, where the x_1' axis is oriented along domain walls, the shear stress $\sigma_{6'}$ vanishes at $\phi^*=0.5$. This demonstrates a decrease in the film elastic energy, which is caused by the domain formation.

The magnitude of spontaneous polarization in the a_1 and a_2 domains depends on the misfit strain and temperature and can be found from the relation

$$P_s^2 = -\frac{\alpha_{11}^{**}}{3\alpha_{111}} + \left(\frac{\alpha_{11}^{**2}}{9\alpha_{111}^2} - \frac{\alpha_1^*}{3\alpha_{111}}\right)^{1/2}, \qquad (8)$$

where $\alpha_1^* = \alpha_1 - (Q_{11}+Q_{12})S_m/(s_{11}+s_{12})$ is the coefficient introduced in Ref. 38, and $\alpha_{11}^{**} = \alpha_{11}+(Q_{11}+Q_{12})^2/[4(s_{11}+s_{12})]$ is the renormalized coefficient of the fourth-order polarization term $(P_1^4 + P_2^4)$ in the free-energy expansion (2), which differs from the similar coefficient α_{11}^* appearing in the theory of single-domain films.[38] The mean energy density $\langle \widetilde{F} \rangle^*(S_m, T, \mathbf{E}_0=0)$ stored in the film with an equilibrium $a_1/a_2/a_1/a_2$ structure is given by

$$\langle \widetilde{F} \rangle^* = \frac{S_m^2}{s_{11}+s_{12}} + \alpha_1^* P_s^2 + \alpha_{11}^{**} P_s^4 + \alpha_{111} P_s^6, \qquad (9)$$

with P_s^2 defined by Eq. (8).

From comparison of Fig. 2(a) with the phase diagram of single-domain PT films,[38] it follows that the $a_1/a_2/a_1/a_2$ polydomain state replaces the orthorhombic aa phase in the equilibrium diagram. Nevertheless, the paraelectric-to-ferroelectric phase transition in our approximation remains to be of the *second order* at positive misfit strains S_m (except for a narrow range near $S_m=0$, where the $c/a/c/a$ state forms). This is due to the fact that the renormalized coefficient α_{11}^{**} is *positive* in PT films, as well as α_{11}^*.

Proceed now to the equilibrium phase diagram of BT films. From inspection of Fig. 2 it can be seen that it has much more complicated structure than the diagram of PT films. The analysis shows that this is due to the existence of three different polarization instabilities in epitaxial BT films. The first one is the P_2 instability of the $c/a/c/a$ polydomain state described in Ref. 36.[51] In contrast with PT films, where this instability appears only in metastable $c/a/c/a$ structures, in BT films it manifests itself in the diagram of equilibrium thermodynamic states leading to the formation of the heterophase $ca^*/aa^*/ca^*/aa^*$ state [see Fig. 3(b)] composed of distorted ca and aa phases.[36]

The second instability refers to the pseudotetragonal $a_1/a_2/a_1/a_2$ state. Under certain S_m-T conditions, this state becomes unstable with respect to the *in-plane rotation* of $\mathbf{P}_s$

away from the edges of the prototypic cubic cell, which leads to its transformation into the orthorhombic aa phase. This instability appears during the film cooling, when the misfit strain S_m in the epitaxial system is larger than about 2 $\times 10^{-3}$. If the misfit strain increases at a given temperature due to the substrate bending, for example, the transformation also should take place at some critical value of S_m (about 5.9×10^{-3} at 25 °C). This behavior may be explained in a natural way because in stress-free BT crystals at temperatures below 10 °C the orthorhombic phase becomes energetically more favorable than the tetragonal one.[40]

The homogeneous aa phase, however, does not appear in the diagram of equilibrium states. The calculations show that it always tends to convert into the polydomain $aa_1/aa_2/aa_1/aa_2$ state, which is energetically more favorable. As a result, well below the transition line $T_c(S_m>0)$ $=T_{aa}(S_m)$, the $aa_1/aa_2/aa_1/aa_2$ domain pattern replaces the $a_1/a_2/a_1/a_2$ one in the equilibrium diagram of BT films [see Fig. 2(b)]. In the $aa_1/aa_2/aa_1/aa_2$ state, the polarization patterning occurs along two in-plane *face diagonals* of the prototypic cubic cell [Fig. 3(e)] so that 90° domain walls form here. The equilibrium volume fractions of the aa_1 and aa_2 domains are equal to each other ($\phi^*=0.5$), and the spontaneous polarization $\mathbf{P}_s$ has the same magnitude in these domains. Internal electric fields and the stresses σ_3, σ_4, σ_5, and σ_6 are absent in the equilibrium $aa_1/aa_2/aa_1/aa_2$ structure. The stresses σ_1 and σ_2 are homogeneous inside the film and, in similarity with the $a_1/a_2/a_1/a_2$ state, have the same value of $\sigma_1=\sigma_2=[S_m-0.5(Q_{11}+Q_{12})P_s^2]/(s_{11}+s_{12})$. The spontaneous polarization can be calculated from the formula

$$P_s^2 = -\frac{2\alpha_{11}^*+\alpha_{12}^{**}}{3(\alpha_{111}+\alpha_{112})} + \left[\frac{(2\alpha_{11}^*+\alpha_{12}^{**})^2}{9(\alpha_{111}+\alpha_{112})^2} - \frac{4\alpha_1^*}{3(\alpha_{111}+\alpha_{112})}\right]^{1/2}, \qquad (10)$$

where $\alpha_{12}^{**}=\alpha_{12}^*-Q_{44}^2/(2s_{44})$, and α_{11}^* and α_{12}^* are the renormalized coefficients of the free-energy expansion, which were introduced in Ref. 38.[52] The mean energy density $\langle \widetilde{F} \rangle^*(S_m, T, \mathbf{E}_0=0)$ in the equilibrium $aa_1/aa_2/aa_1/aa_2$ polydomain state can be found from the relation

$$\langle \widetilde{F} \rangle^* = \frac{S_m^2}{s_{11}+s_{12}} + \alpha_1^* P_s^2 + \frac{1}{4}(2\alpha_{11}^*+\alpha_{12}^{**})P_s^4$$
$$+ \frac{1}{4}(\alpha_{111}+\alpha_{112})P_s^6, \qquad (11)$$

where P_s^2 is given by Eq. (10).

The third instability, which exists in epitaxial BT films, is the instability of the $a_1/a_2/a_1/a_2$ and $aa_1/aa_2/aa_1/aa_2$ states with respect to the *appearance* of the polarization component P_3 orthogonal to the film surfaces. This P_3 instability occurs below the Curie-Weiss temperature $\theta=108$ °C of bulk BT crystals, when the magnitude of the positive misfit strain in the film/substrate system *decreases* down to some

critical value. It also appears during the film cooling under certain misfit-strain conditions.

Owing to the P_3 instability, the $a_1/a_2/a_1/a_2$ and $aa_1/aa_2/aa_1/aa_2$ configurations transform into *new* polydomain states, which may be termed $ca_1/ca_2/ca_1/ca_2$ and $r_1/r_2/r_1/r_2$ structures, respectively. In both states, the out-of-plane polarizations in neighboring domains have opposite directions but the same magnitude ($P_3'=-P_3''$), whereas the in-plane polarizations retain the orientations characteristic of the $a_1/a_2/a_1/a_2$ and $aa_1/aa_2/aa_1/aa_2$ configurations [see Figs. 3(d) and 3(f)]. Since in the $ca_1/ca_2/ca_1/ca_2$ pattern the spontaneous polarizations are parallel to the out-of-plane *faces* of the prototypic cubic cell, it may be regarded as a polydomain analogue of the monoclinic ca phase forming in single domain BT films.[38] In the $r_1/r_2/r_1/r_2$ state, the in-plane polarizations are oriented along the face *diagonals* of the prototypic cell so that the spatial orientation of $\mathbf{P}_s$ here is similar to that in the homogeneous monoclinic r phase.[38] The equilibrium volume fractions of the r_1 and r_2 domains are equal to each other ($\phi^*=0.5$), as well as the populations of the ca_1 and ca_2 domains.

Remarkably, the spatial orientations of the spontaneous polarization $\mathbf{P}_s$ in the $ca_1/ca_2/ca_1/ca_2$ and $r_1/r_2/r_1/r_2$ states depend on the misfit strain S_m and temperature T. Therefore, the vector $\mathbf{P}_s$ generally is not parallel to the face or cube diagonals of the prototypic cell [Figs. 3(d) and 3(f)] so that these two states have no direct analogue in bulk BT crystals. The domain walls in these patterns are not 90° walls anymore. Since the rotation of $\mathbf{P}_s$ at the ca_1/ca_2 wall is larger than 90°, but generally not equal to 120°, this wall differs from 120° domain boundaries in the orthorhombic phase of a bulk BT crystal. The r_1/r_2 walls are not equivalent to the domain walls in the stress-free rhombohedral BT crystal as well. Nevertheless, the presence of the $r_1/r_2/r_1/r_2$ pattern in the (S_m,T) diagram has probably the same origin as the formation of the rhombohedral phase in bulk BT crystals at $T<-71$ °C.[40–41]

Thus, in BT films, the stability range of polydomain states with walls orthogonal to the substrate splits into four parts. These parts are separated by the first-order transition lines and correspond to the $a_1/a_2/a_1/a_2$, $aa_1/aa_2/aa_1/aa_2$, $ca_1/ca_2/ca_1/ca_2$, and $r_1/r_2/r_1/r_2$ configurations.

Finally, it should be noted that there are some similarities between the phase diagrams of BT and PT films. For example, the transition line between the homogeneous c phase and the $c/a/c/a$ state is defined in BT by the relationships discussed above for PT films. In both PT and BT, this line contains a special point, at which the continuous (in our approximation) transition becomes a discontinuous one. Such "tricritical" point also exists in BT films on the transition line $T_{aa}(S_m)$ between the paraelectric phase and the $a_1/a_2/a_1/a_2$ state [see Fig. 2(d)].

IV. DIELECTRIC PROPERTIES OF POLYDOMAIN FERROELECTRIC FILMS

In general, the dielectric response of a polydomain or heterophase film is a sum of *intrinsic* and *extrinsic* contributions. Changes of the polarizations $\mathbf{P}',\mathbf{P}''$ inside dissimilar domains (phase layers) lead to an average intrinsic (volume) response. If the measuring field $\mathbf{E}_0$ also induces reversible displacements of domain walls (phase boundaries) from their initial equilibrium positions, an additional extrinsic contribution may appear, being caused by rotations of the polarization vector in the part of the film volume swept by moving walls.[27,28] Fortunately, our thermodynamic theory makes it possible to calculate the *total permittivity* of a polydomain or heterophase film, which results from both intrinsic and extrinsic contributions. To that end, equilibrium polarizations $\mathbf{P}',\mathbf{P}''$ in the domains (phase layers) of two types and their equilibrium volume fractions should be determined numerically as a function of the external electric field $\mathbf{E}_0$. Then the permittivity of a ferroelectric film can be found from the field dependence of the average polarization $\langle\mathbf{P}\rangle=\phi^*\mathbf{P}'+(1-\phi^*)\mathbf{P}''$ in an epitaxial layer. Choosing a reasonable magnitude E_0 of the weak external field, we calculated the small-signal dielectric constants $\varepsilon_{ij}(i,j=1,2,3)$ of PT and BT films from the relation

$$\varepsilon_{ij}=\frac{\langle P_i\rangle(E_{0j}=E_0)-\langle P_i\rangle(E_{0j}=0)}{E_0}. \qquad (12)$$

Since the equilibrium domain population ϕ^* was allowed to vary under field $\mathbf{E}_0$, the constants ε_{ij} involved a nonzero extrinsic (domain-wall) contribution when the projection of the spontaneous polarization on $\mathbf{E}_0$ was different in dissimilar domains. The calculated constants also correctly take into account the influence of the mechanical film/substrate interaction on the intrinsic (volume) responses of the domains of two types.

Figure 4 shows variations of the diagonal components of the dielectric tensor ε_{ij} with the misfit strain S_m in PT films at room temperature. At the transition point $S_m^0(T=25\,°C)=-14.7\times10^{-3}$, where the transformation of the c phase into the $c/a/c/a$ pattern takes place, finite jumps of ε_{11} and ε_{33} occur, while the dependence $\varepsilon_{22}(S_m)$ only changes its slope. The analysis shows that the steplike increase of ε_{11} and ε_{33} at $S_m=S_m^0$ is entirely due to the appearance of domain-wall contributions to these dielectric constants in the polydomain $c/a/c/a$ state. If domain walls are assumed to be pinned so that the domain population $\phi(\mathbf{E}_0)$ is kept fixed at a value of $\phi^*(\mathbf{E}_0=0)$ during the calculations, all constants ε_{ii} vary in a continuous manner on crossing the transition line (see dashed lines in Fig. 4). The slope of $\varepsilon_{33}(S_m)$ changes slightly here, whereas $\varepsilon_{11}(S_m)$ has a cusplike anomaly at $S_m=S_m^0$. Such dielectric behavior can be attributed to the fact that the formation of the polydomain $c/a/c/a$ state in our approximation proceeds via the introduction of a small volume fraction of the a domains (with a finite spontaneous polarization P_0) into the c phase.

It should be noted that the theoretical domain-wall contribution $\Delta\varepsilon_{33}/\varepsilon_0$ to the film permittivity ε_{33}, which is measured in a conventional plate-capacitor setup, increases from 70 to 120 in the range of misfit strains between -14.7×10^{-3} and 4.6×10^{-3}, where the $c/a/c/a$ pattern represents the most energetically favorable configuration. These values may be compared with the results of approximate analytical
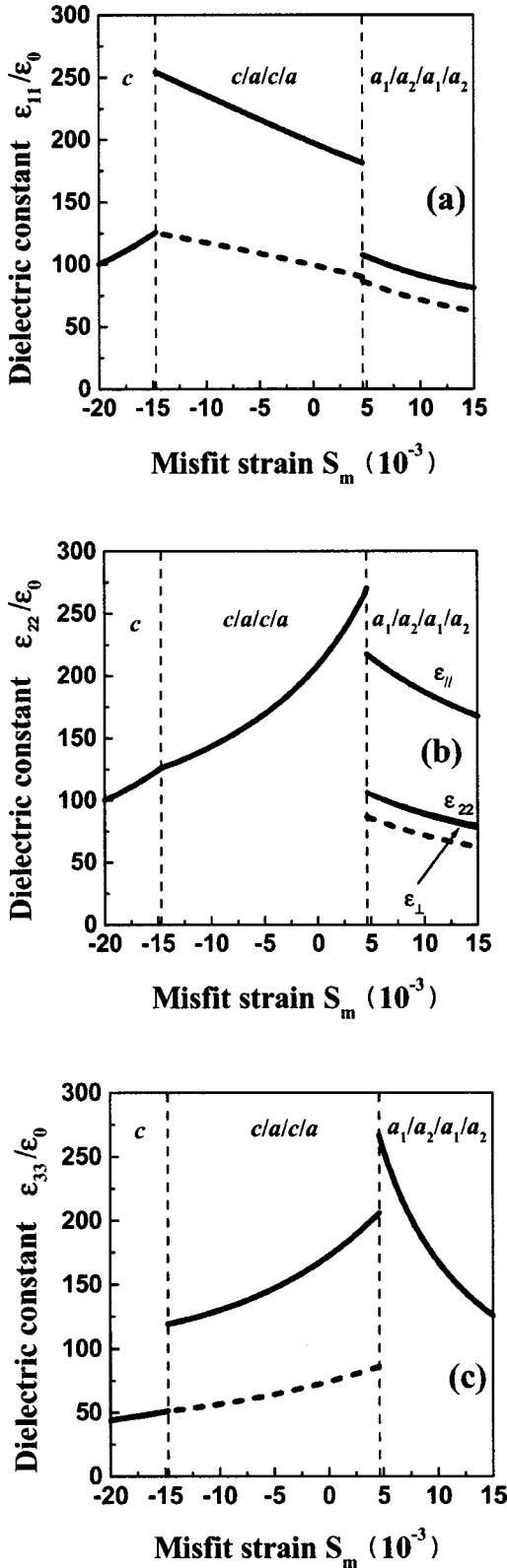
FIG. 4. Dependences of the dielectric constants ε_{11} (a), ε_{22} (b), and ε_{33} (c) of PbTiO$_3$ films on the misfit strain S_m at $T = 25\,°C$. The dashed lines show the permittivities of PbTiO$_3$ films with pinned domain walls. For films with the $a_1/a_2/a_1/a_2$ domain structure, the in-plane dielectric responses $\varepsilon_{\parallel}$ and $\varepsilon_{\perp}$ in the directions parallel and orthogonal to the 90° walls are also shown for comparison.

calculations of $\Delta\varepsilon_{33}$, which can be performed in the framework of our theory as well. In the first approximation, the effect of small domain-wall displacements on the polarizations $\mathbf{P}', \mathbf{P}''$ inside c and a domains may be neglected. Evaluating in this approximation the field-induced change of the domain population ϕ via the mathematical procedure developed in Sec. II, from Eq. (12) we obtain

$$\Delta\varepsilon_{33} \approx \frac{(s_{11}^2 - s_{12}^2)}{s_{11}(Q_{11} - Q_{12})^2 P_s^2}. \qquad (13)$$

Equation (13) is similar to an analytic expression, which was derived for $\Delta\varepsilon_{33}$ earlier in the approximation of the linear isotropic theory of elasticity.[27,28] The substitution of Eq. (4) for the spontaneous polarization P_s into Eq. (13) gives $\Delta\varepsilon_{33}/\varepsilon_0 \approx 110$–$130$ for PT films at room temperature, which is in reasonable agreement with our numerical results. Though the linear approximation overestimates $\Delta\varepsilon_{33}$, the main conclusion made in Refs. 27 and 28 is justified by the nonlinear theory. Indeed, according to our calculations, the domain-wall contribution $\Delta\varepsilon_{33}$ represents more than a half of the total response of a polydomain PT film so that translational displacements of 90° walls really contribute considerably to the film permittivity. [As demonstrated by Fig. 5(c), a similar situation takes place in BT films with the equilibrium $c/a/c/a$ domain structure. Here the domain-wall contribution $\Delta\varepsilon_{33}/\varepsilon_0$ varies between 375 and 387, which may be compared with $\Delta\varepsilon_{33}/\varepsilon_0 \approx 510$–$530$ given by the linear theory.]

When the misfit strain in the heterostructure increases above a value of $S_m = 4.6 \times 10^{-3}$, the $a_1/a_2/a_1/a_2$ polydomain state replaces the $c/a/c/a$ one in the phase diagram of PT films. At this threshold strain, as may be expected, the film dielectric constants ε_{ii} exhibit steplike changes (see Fig. 4). Remarkably, in the vicinity of the threshold strain the permittivity ε_{33} of an epitaxial PT film becomes considerably higher than the largest dielectric constant of a single-domain bulk PT crystal. (According to the thermodynamic calculations, the latter is about 125 at room temperature.)

For films with the $a_1/a_2/a_1/a_2$ domain pattern, the dielectric response ε_{33} in the film-thickness direction can be calculated analytically. In this case the domain-wall contribution is absent and the inverse dielectric susceptibility χ_{33} equals

$$\chi_{33} = 2\alpha_3^* + 2\alpha_{13}^{**} P_s^2 + 2\alpha_{112} P_s^4, \qquad (14)$$

where $\alpha_3^* = \alpha_1 - S_m 2Q_{12}/(s_{11} + s_{12})$ is the coefficient introduced in Ref. 38, and $\alpha_{13}^{**} = \alpha_{12} + (Q_{11} + Q_{12})Q_{12}/(s_{11} + s_{12}) + Q_{44}^2/(4s_{44})$ is the renormalized coefficient of the fourth-order polarization term $(P_1^2 + P_2^2)P_3^2$ in the free-energy expansion (2), which differs from the similar coefficient α_{13}^* appearing in the theory of single-domain ferroelectric films, i.e., $\alpha_{13}^{**} = \alpha_{13}^* + Q_{44}^2/(4s_{44})$. The substitution of Eq. (8) into Eq. (14) makes it possible to calculate $\varepsilon_{33} = \varepsilon_0 + \chi_{33}^{-1}$ as a function of the misfit strain and temperature.

The in-plane dielectric responses ε_{11} and ε_{22} of a film with the $a_1/a_2/a_1/a_2$ structure, measured along the [100] and [010] crystallographic axes, are equal to each other and

contain a nonzero domain-wall contribution [see Figs. 4(a) and 4(b)]. This contribution appears because the electric field is directed at 45° to the 90° walls [see Fig. 1(b)]. For comparison, we also calculated the film in-plane permittivities $\varepsilon_\perp$ and $\varepsilon_\parallel$ in the directions orthogonal and parallel to the a_1/a_2 domain walls. When the measuring field $\mathbf{E}_0$ is orthogonal to the walls, there is no driving force acting on them and the domain-wall contribution to the corresponding permittivity $\varepsilon_\perp$ equals zero. In contrast, the field $\mathbf{E}_0$ oriented along a_1/a_2 walls in the film plane induces the wall displacements from equilibrium positions so that the dielectric response $\varepsilon_\parallel$ should contain a nonzero domain-wall contribution $\Delta\varepsilon_\parallel$. From inspection of Fig. 4(b), it can be seen that $\varepsilon_\parallel$ is about 2 times larger than $\varepsilon_\perp$.

Let us discuss now peculiarities of the dielectric properties of BT films. The misfit-strain dependences of the film permittivities ε_{ii} at room temperature are shown in Fig. 5. As may be expected, the polarization instabilities of polydomain states, which were described in Sec. III, manifest itself in strong dielectric anomalies. The transition between the $c/a/c/a$ and $ca^*/aa^*/ca^*/aa^*$ states is accompanied by a singularity of ε_{22}, which is caused by the P_2 instability. A sharp peak of ε_{33} is associated with the P_3 instability of the $a_1/a_2/a_1/a_2$ pattern, which leads to the formation of the $ca_1/ca_2/ca_1/ca_2$ configuration. On the other hand, the instability of the $a_1/a_2/a_1/a_2$ state with respect to the in-plane rotation of the spontaneous polarization does not manifest itself in Fig. 5. This is due to the fact that the critical misfit strain $S_m=5.89\times10^{-3}$ for this instability is considerably larger than the strain $S_m=3.65\times10^{-3}$, at which the $aa_1/aa_2/aa_1/aa_2$ pattern replaces the $a_1/a_2/a_1/a_2$ structure in the equilibrium phase diagram. At the transition between these two in-plane polarization states, the dielectric constants ε_{ii} experience only steplike changes.

The dielectric response ε_{33} of the film with the $aa_1/aa_2/aa_1/aa_2$ domain pattern can be found analytically, because it does not contain the domain-wall contribution. For the inverse dielectric susceptibility χ_{33}, the calculation yields

$$\chi_{33}=2\alpha_3^*+2\alpha_{13}^{**}P_s^2+\left(\alpha_{112}+\frac{1}{2}\alpha_{123}\right)P_s^4, \qquad (15)$$

where P_s^2 given by Eq. (10) should be substituted. The permittivity $\varepsilon_{33}=\varepsilon_0+\chi_{33}^{-1}$ increases with decreasing positive misfit strain, as demonstrated by Fig. 5(c).

In conclusion of this section we analyze domain-wall contributions to the in-plane dielectric responses ε_{11} and ε_{22} of polydomain ferroelectric films, which could be measured in setups with interdigitated surface electrodes. For films with the $c/a/c/a$ structure, the domain-wall contribution $\Delta\varepsilon_{11}$ calculated in the linear approximation is equal to the contribution $\Delta\varepsilon_{33}$ by reason of symmetry. Using Eq. (13), we obtain $\Delta\varepsilon_{11}/\varepsilon_0\approx110-130$ and $510-530$ for PT and BT films, respectively. These estimates are in good agreement with the results of our numerical calculations, which give $\Delta\varepsilon_{11}/\varepsilon_0$ between 130 and 90 for PT films and between 600 and 580 for BT ones [see Figs. 4(a) and 5(a)].
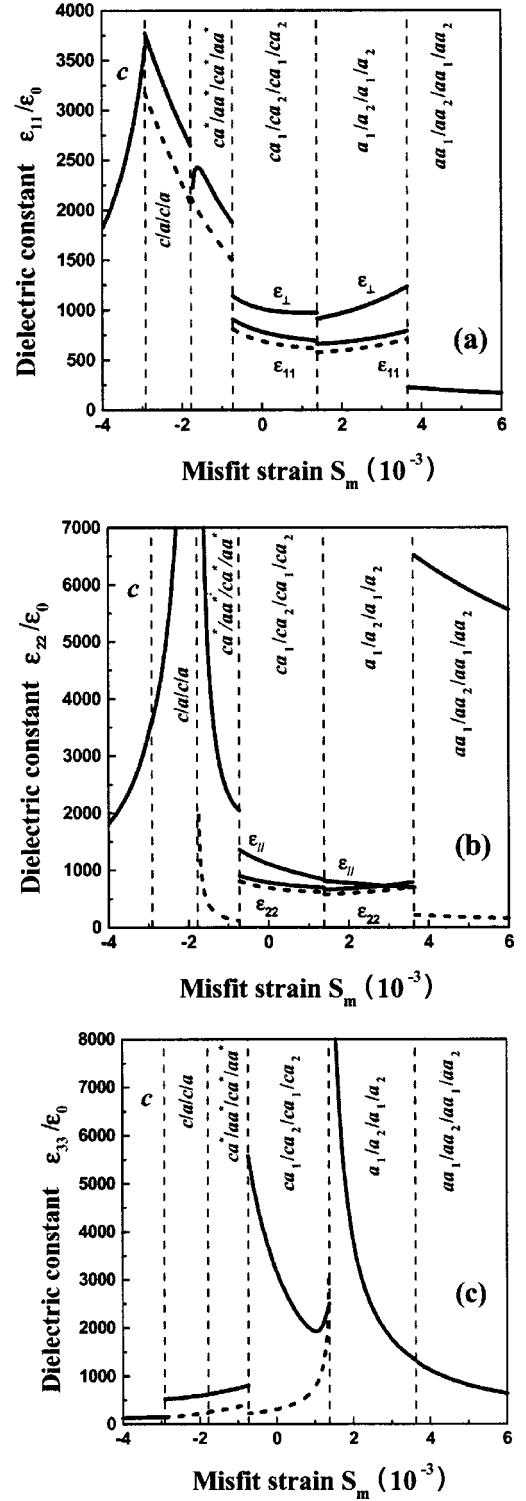

FIG. 5. Permittivities of BaTiO$_3$ epitaxial thin films as functions of the misfit strain S_m at $T=25$ °C: ε_{11} (a), ε_{22} (b), and ε_{33} (c). The dashed lines show the dielectric constants of BaTiO$_3$ films with pinned domain walls. For films with the $a_1/a_2/a_1/a_2$ and $ca_1/ca_2/ca_1/ca_2$ domain structures, the in-plane dielectric responses $\varepsilon_\parallel$ and $\varepsilon_\perp$ in the directions parallel and orthogonal to the domain walls are also shown for comparison.

The domain-wall contributions to the dielectric constants of ferroelectric films with the $a_1/a_2/a_1/a_2$ and $aa_1/aa_2/aa_1/aa_2$ structures can be evaluated in the linear approximation by analogy with the derivation of Eq. (13). Neglecting polarization changes accompanying the field-induced displacements of 90° walls from their initial positions, we obtain

$$\Delta\varepsilon_{11} = \Delta\varepsilon_{22} \approx \frac{(s_{11} - s_{12})}{2(Q_{11} - Q_{12})^2 P_s^2} \qquad (16)$$

for the $a_1/a_2/a_1/a_2$ state and

$$\Delta\varepsilon_{22} \approx \frac{2s_{44}}{Q_{44}^2 P_s^2} \qquad (17)$$

for the $aa_1/aa_2/aa_1/aa_2$ one. The substitution of Eq. (10) for the spontaneous polarization P_s into Eq. (17) shows that in BT films with the equilibrium $aa_1/aa_2/aa_1/aa_2$ structure $\Delta\varepsilon_{22}/\varepsilon_0 \approx 6500$ at the threshold misfit strain $S_m = 3.65 \times 10^{-3}$, in good agreement with the contribution $\Delta\varepsilon_{22}/\varepsilon_0 = 6300$ calculated numerically. In the case of the $a_1/a_2/a_1/a_2$ domain configuration, from Eqs. (8) and (16) we obtain $\Delta\varepsilon_{11}/\varepsilon_0 \approx 110$ for PT films at $S_m = 4.6 \times 10^{-3}$ and $\Delta\varepsilon_{11}/\varepsilon_0 \approx 400$ for BT films at $S_m = 1.38 \times 10^{-3}$, for example. According to our numerical calculations, the contribution $\Delta\varepsilon_{11}/\varepsilon_0$ equals 20 and 80 in these two situations, respectively. It can be seen that the linear approximation strongly overestimates the domain-wall contribution to the dielectric response in this particular case.

V. PIEZOELECTRIC RESPONSE OF POLYDOMAIN FERROELECTRIC FILMS

In this section the piezoelectric properties of polydomain ferroelectric thin films epitaxially grown on thick cubic substrates will be described. We restrict our study to the converse piezoelectric effect, which consists in changes of the film dimensions and shape under the action of an external electric field $\mathbf{E}_0$.

The small-signal piezoelectric coefficients d_{in} characterizing this effect can be found from the field dependence of the mean strains $\langle S_n \rangle = \phi^* S_n' + (1 - \phi^*) S_n''$ in a polydomain film as

$$d_{in} = \frac{\langle S_n \rangle (E_{0i} = E_0) - \langle S_n \rangle (E_{0i} = 0)}{E_0}. \qquad (18)$$

Since the epitaxial film is rigidly connected with a thick substrate, which is assumed to be piezoelectrically inactive, the strains $\langle S_1 \rangle$, $\langle S_2 \rangle$, and $\langle S_6 \rangle$ cannot change under the field so that $d_{i1} = d_{i2} = d_{i6} = 0$. Variations of the strains $\langle S_3 \rangle$, $\langle S_4 \rangle$, and $\langle S_5 \rangle$ manifest itself in a change of the film thickness and a tilt of the ferroelectric overlayer relative to the substrate normal. These strains can be expressed in terms of polarization components in the domains of two types and the relative domain population ϕ as
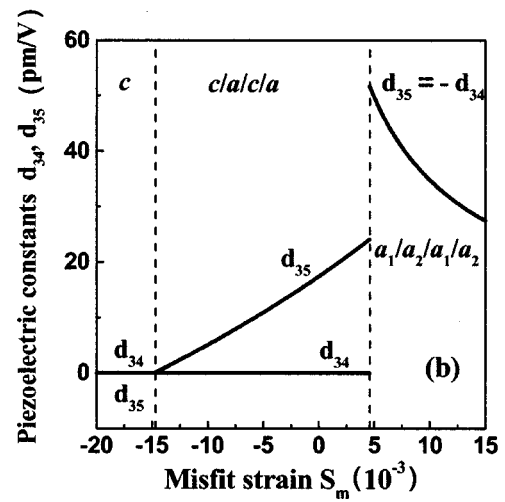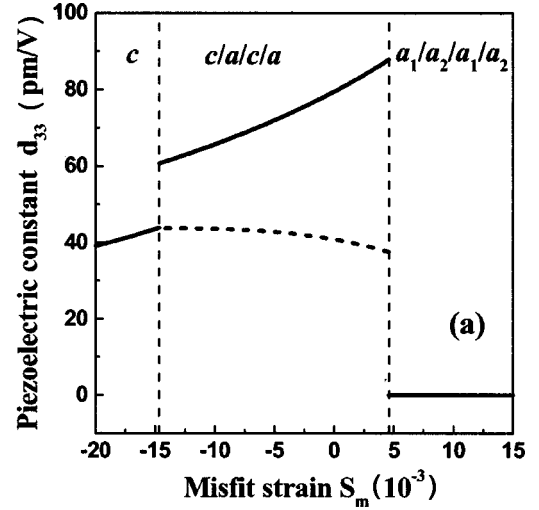

FIG. 6. Dependences of the piezoelectric coefficients d_{33} (a) and d_{34}, d_{35} (b) of PbTiO$_3$ films on the misfit strain S_m at $T = 25\,°$C. The dashed line shows the piezoelectric response d_{33} of PbTiO$_3$ films with pinned domain walls.

$$\langle S_3 \rangle = \frac{2s_{12}}{s_{11} + s_{12}} S_m + \frac{Q_{12}s_{11} - Q_{11}s_{12}}{s_{11} + s_{12}} [\phi(P_1'^2 + P_2'^2) + (1 - \phi)(P_1''^2 + P_2''^2)]$$
$$+ \left(Q_{11} - \frac{2Q_{12}s_{12}}{s_{11} + s_{12}}\right)[\phi P_3'^2 + (1 - \phi)P_3''^2], \qquad (19)$$

$$\langle S_4 \rangle = Q_{44}[\phi P_2' P_3' + (1 - \phi)P_2'' P_3''], \qquad (20)$$

$$\langle S_5 \rangle = Q_{44}[\phi P_1' P_3' + (1 - \phi)P_1'' P_3'']. \qquad (21)$$

In a conventional plate-capacitor setup, where the film is sandwiched between two continuous electrodes, the piezoelectric measurements give the coefficients d_{33}, d_{34}, and d_{35}. Using Eq. (18), we calculated numerically these piezoelectric constants for PT and BT films with equilibrium domain structures. Figures 6 and 7 show the theoretical misfit-strain dependences of d_{33}, d_{34}, and d_{35} at room temperature.
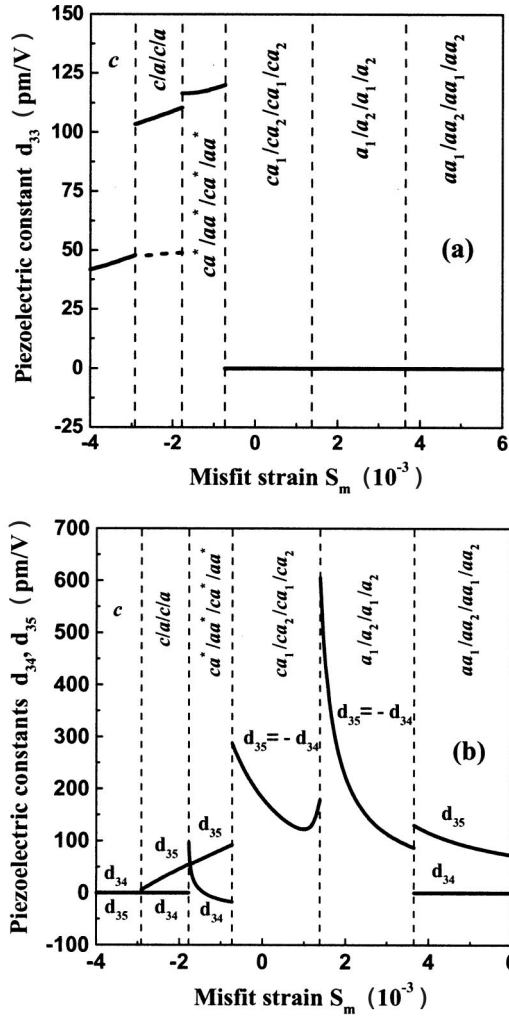
FIG. 7. Piezoelectric coefficients of BaTiO$_3$ films as functions of the misfit strain S_m at $T=25\,°C$: d_{33} (a), d_{34}, d_{35} (b). The dashed line shows the piezoelectric response d_{33} of BaTiO$_3$ films with pinned domain walls calculated for the $c/a/c/a$ state.

From inspection of Fig. 6(a) it can be seen that the longitudinal piezoelectric coefficient d_{33} of PT films increases with the increase of the misfit strain S_m up to the threshold strain $S_m=4.6\times10^{-3}$, at which the $c/a/c/a$ polydomain state is replaced by the $a_1/a_2/a_1/a_2$ one. A similar trend is characteristic of the misfit-strain dependence of d_{33} in BT films, where the maximum response is displayed by a film with the $ca^*/aa^*/ca^*/aa^*$ structure [see Fig. 7(a)]. It should be noted that these theoretical results correspond to the properties of prepolarized ferroelectric films, where all 180° domain walls are removed prior to the piezoelectric measurements.

The steplike increase of the constant d_{33} at the transition from the c phase to the $c/a/c/a$ state is due to the appearance of a nonzero domain-wall contribution Δd_{33} [see Figs. 6(a) and 7(a)]. Within the stability range of the $c/a/c/a$ structure, the value of Δd_{33} varies from 17 to 50 pm/V in PT films and between 56 and 61 pm/V in BT films. These values may be compared with the domain-wall contribution Δd_{33} calculated for dense domain structures with the aid of the

linear theory.[31] Using the relation derived in Ref. 31 and taking into account the elastic anisotropy of the paraelectric phase, we obtain

$$\Delta d_{33} = \frac{(s_{11}+2s_{12})(s_{11}-s_{12})}{s_{11}(Q_{11}-Q_{12})P_0}. \tag{22}$$

For PT and BT films at room temperature, Eq. (22) gives Δd_{33} about 45 and 95 pm/V, respectively. These values are in reasonable agreement with the aforementioned results of our calculations. Though the linear approximation overestimates Δd_{33}, the earlier prediction[31] that the displacements of 90° domain walls may contribute considerably to the longitudinal piezoelectric response of polydomain ferroelectric thin films is confirmed by the nonlinear thermodynamic theory [see Figs. 6(a) and 7(a)].

The numerical calculations also show that ferroelectric films with the equilibrium $a_1/a_2/a_1/a_2$, $aa_1/aa_2/aa_1/aa_2$, and $ca_1/ca_2/ca_1/ca_2$ domain structures have a negligible piezoelectric coefficient d_{33}. When the field-induced displacements of domain walls are absent, as in the $a_1/a_2/a_1/a_2$ and $aa_1/aa_2/aa_1/aa_2$ states, from Eqs. (18) and (19) it follows that the piezoelectric response d_{33} can be written as

$$\begin{aligned} d_{33} = 2\,\frac{Q_{12}s_{11}-Q_{11}s_{12}}{s_{11}+s_{12}}[\,\phi(\eta'_{13}P'_1+\eta'_{23}P'_2) \\ +(1-\phi)(\eta''_{13}P''_1+\eta''_{23}P''_2)] \\ +2\left(Q_{11}-\frac{2Q_{12}s_{12}}{s_{11}+s_{12}}\right)[\,\phi\eta'_{33}P'_3+(1-\phi)\eta''_{33}P''_3], \end{aligned} \tag{23}$$

where η'_{ij} and η''_{ij} are the intrinsic dielectric susceptibilities of the ferroelectric material inside domains of the first and second kinds, respectively. Equation (23) demonstrates that the piezoelectric response d_{33} of the $a_1/a_2/a_1/a_2$ and $aa_1/aa_2/aa_1/aa_2$ states must be really very small. Indeed, in these states at $\mathbf{E}_0=0$ only the in-plane polarization differs from zero, which is multiplied by nondiagonal components of the dielectric tensor η_{ij} in the expression for d_{33}. The fact that films with the $ca_1/ca_2/ca_1/ca_2$ structure have a negligible coefficient d_{33} may be explained by the zero value of the average out-of-plane polarization P_3 in this state as well.

Consider now the misfit-strain dependences of the piezoelectric coefficients d_{34} and d_{35} in epitaxial PT and BT films [Figs. 6(b) and 7(b)]. By reason of symmetry $d_{34}=d_{35}=0$ in the c phase and $d_{34}=0$ in the $c/a/c/a$ state. The piezoelectric response d_{35} increases with the misfit strain S_m in films with the $c/a/c/a$ and $ca^*/aa^*/ca^*/aa^*$ structures. In contrast, the coefficient d_{34} displayed by the $ca^*/aa^*/ca^*/aa^*$ state decreases and even changes sign, as the magnitude of $S_m<0$ is reduced for BT films. The nonmonotonic variation of $d_{34}=-d_{35}$ in BT films having the $ca_1/ca_2/ca_1/ca_2$ structure is similar to the behavior of the dielectric constant ε_{33} here [see Fig. 5(c)]. Of course, the calculated piezoelec-

tric responses d_{3n} of the $c/a/c/a$, $ca*/aa*/ca*/aa*$, and $ca_1/ca_2/ca_1/ca_2$ states involve a nonzero domain-wall contribution.

If the relative domain population ϕ does not change during piezoelectric measurements, Eqs. (20) and (21) yield the following relations for the coefficients d_{34} and d_{35}:

$$d_{34} = Q_{44}[\phi(\eta'_{23}P'_3 + \eta'_{33}P'_2) + (1-\phi)(\eta''_{23}P''_3 + \eta''_{33}P''_2)],$$
(24)

$$d_{35} = Q_{44}[\phi(\eta'_{13}P'_3 + \eta'_{33}P'_1) + (1-\phi)(\eta''_{13}P''_3 + \eta''_{33}P''_1)].$$
(25)

For the $a_1/a_2/a_1/a_2$ and $aa_1/aa_2/aa_1/aa_2$ polydomain states, where $P'_3 = P''_3 = 0$ at $\mathbf{E}_0 = 0$ and $\eta'_{33} = \eta''_{33} = \eta_{33}$, from Eqs. (24) and (25) we obtain $d_{34} = Q_{44}\eta_{33}\langle P_2 \rangle$ and $d_{35} = Q_{44}\eta_{33}\langle P_1 \rangle$. These relations explain some peculiarities of the piezoelectric behavior revealed by numerical calculations [Figs. 6(b) and 7(b)]. Indeed, they show that in films with the $a_1/a_2/a_1/a_2$ domain structure the equality $d_{34} = -d_{35}$ must hold since $\langle P_1 \rangle = -\langle P_2 \rangle$ at the orientation of the a_1/a_2 walls shown in Fig. 1(b). In the case of the $aa_1/aa_2/aa_1/aa_2$ polydomain state, the piezoelectric response d_{34} is absent because the average polarization in the [010] direction equals zero ($\langle P_2 \rangle = 0$) for the chosen domain geometry [Fig. 1(c)]. The reduction of the piezoelectric constant d_{35} with increasing misfit strain S_m in films with the $a_1/a_2/a_1/a_2$ and $aa_1/aa_2/aa_1/aa_2$ structures can be attributed to the decrease of the dielectric susceptibility η_{33} here [see Figs. 4(c) and 5(c)]. The jump of d_{35} at the transition from the $a_1/a_2/a_1/a_2$ to $aa_1/aa_2/aa_1/aa_2$ state in BT films is mainly due to a larger average polarization $\langle P_1 \rangle$ in the latter.

VI. CONCLUDING REMARKS

The nonlinear thermodynamic theory developed in this paper makes it possible to include laminar polydomain states into the misfit strain-temperature phase diagrams of epitaxial ferroelectric thin films and to determine the total dielectric and piezoelectric responses of polydomain films. Our calculations revealed several important features of the polydomain (twinned) states in epitaxial films of perovoskite ferroelectrics. In particular, the phase diagram of BT films was found to be much more complicated than the diagram of PT films (see Fig. 2). This distinction reflects the existence of three different ferroelectric phases (tetragonal, orthorhombic, and rhombohedral) in stress-free bulk BT crystals instead of only one (tetragonal) in PT crystals.

Surprisingly, the *direct transformation* of the paraelectric phase into the polydomain $c/a/c/a$ state was shown to take place in PT films only in a narrow misfit-strain range near $S_m = 0$ [Fig. 2(c)]. Usually, the formation of the $c/a/c/a$ domain structure should proceed via a *two-stage process*.

At negative misfit strains, this process involves the appearance of the homogeneous ferroelectric c phase in the first stage followed by the nucleation of a domains inside this out-of-plane polarization state. In our approximation, the transformation of the c phase into the $c/a/c/a$ pattern, which occurs along the thin line shown in Fig. 2(a), appears to be
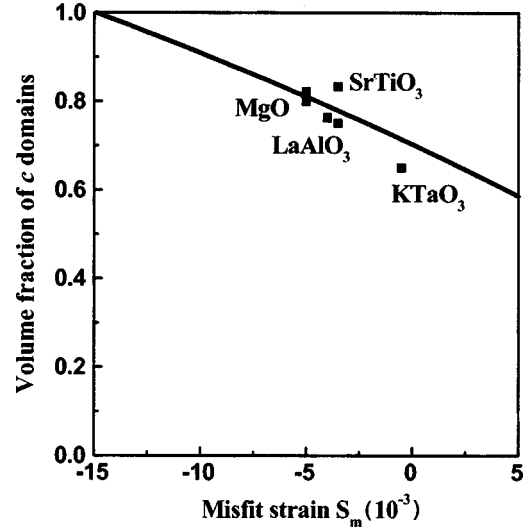

FIG. 8. Misfit-strain dependence of the volume fraction ϕ_c of c domains in thick PbTiO$_3$ epitaxial films at $T = 25\,°C$. The solid line gives the calculated fraction ϕ_c. The squares show the values observed for films grown on various substrates indicated in the figure. The experimental data are taken from Refs. 11, 14 (MgO), 14 (LaAlO$_3$), 12, 14 (SrTiO$_3$), and 2 (KTaO$_3$). The misfit strains for corresponding heterostructures were calculated as described in Ref. 39 by using the following values of the thermal expansion coefficients: $5.5 \times 10^{-6}\,K^{-1}$ (PT), $11 \times 10^{-6}\,K^{-1}$ (SrTiO$_3$ and LaAlO$_3$) (Ref. 53) $14.8 \times 10^{-6}\,K^{-1}$ (MgO), and $6.67 \times 10^{-6}\,K^{-1}$ (KTaO$_3$) (Ref. 6).

continuous in the sense that the volume fraction $\phi_a = 1 - \phi_c$ of a domains gradually increases from zero on crossing the transition line $S_m^0(T)$. This is, however, not exactly correct because we have neglected the self-energies of domain walls in our calculations. Strictly speaking, the discussed transition is discontinuous, and a small but finite ϕ_a appears at the actual transition line, slightly shifted towards lower temperatures from the thin line drawn in Fig. 2(a).

The nucleation of embedded a domains in the c phase during the cooling must be a thermally activated process so that a certain time is required for the formation of an equilibrium $c/a/c/a$ pattern. Therefore, the observed populations of c and a domains in an epitaxial film may depend strongly on the cooling rate dT/dt. Slow cooling rates are expected to facilitate larger volume fractions ϕ_a to be observed at room temperature. In contrast, at very high rates dT/dt the complete suppression of domain formation may take place so that the metastable c phase becomes frozen in. Accordingly, our theory gives a natural explanation for the experimental results obtained in Refs. 5 and 14 on the effect of cooling rate on domain populations in epitaxial PbZr$_{0.20}$Ti$_{0.80}$O$_3$ and PT thin films. This explanation differs considerably from the one proposed earlier by Speck *et al.* on the basis of the linear domain theory.[7]

At positive misfit strains, the $c/a/c/a$ structure is expected to form via the nucleation of c domains inside an in-plane polarization state already existing in the film. The equilibrium volume fraction of c domains, according to Eq. (5), must increase during the film cooling in this case. The

critical temperature $T_{a \to c/a}$, at which the c domains begin to form in a film, may be well below the Curie-Weiss temperature $\theta = 479\,^{\circ}\text{C}$ of the bulk PT. Both these features were observed in PT films grown on (001)-oriented MgO by Lee and Baik, who used the synchrotron x-ray diffraction to measure the domain populations.[17] It should be emphasized that the critical temperature $T_{a \to c/a}$ may be much lower than the actual temperature of the ferroelectric phase transition T_{aa}, which is always higher than θ.

Finally, we would like to stress that our theoretical predictions on the geometry of the dense $c/a/c/a$ structure agree with the experimental data available for sufficiently thick PT films ($H \gtrsim 100\,\text{nm}$). Figure 8 compares the misfit-strain dependence of the volume fraction ϕ_c of c domains, calculated from Eqs. (4) and (5), and the measured values of ϕ_c. Good agreement between the theory and experiment supports the validity of the stability range R_d, which has

been predicted in this paper for the $c/a/c/a$ polydomain state in the (S_m, T) phase diagram. Unfortunately, we are not aware of experimental data on the dielectric and piezoelectric properties of polydomain single-crystalline ferroelectric films. At the same time, the calculated dielectric constant $\varepsilon_{33}/\varepsilon_0 \approx 170$ and piezoelectric coefficient $d_{33} \approx 80\,\text{pm/V}$ of PT films near $S_m = 0$ are in order-of-magnitude agreement with the measured responses of polycrystalline PT films grown on platinum coated silicon substrates ($\varepsilon_{33}/\varepsilon_0 \approx 100$ and $d_{33} \approx 50\,\text{pm/V}$).[54]

*Electronic address: pertsev@domain.ioffe.rssi.ru

[1] A. L. Roitburd, Phys. Status Solidi A **37**, 329 (1976).

[2] B. S. Kwak, A. Erbil, B. J. Wilkens, J. D. Budai, M. F. Chisholm, and L. A. Boather, Phys. Rev. Lett. **68**, 3733 (1992).

[3] Y. Gao, G. Bai, K. L. Merkle, Y. Shi, H. L. M. Chang, Z. Chen, and D. J. Lam, J. Mater. Res. **8**, 145 (1993).

[4] A. E. M. De Veirman, J. Timmers, F. J. G. Hakkens, J. F. M. Cillessen, and R. M. Wolf, Philips J. Res. **47**, 185 (1993).

[5] R. Ramesh, T. Sands, and V. G. Keramidas, Appl. Phys. Lett. **63**, 731 (1993).

[6] B. S. Kwak, A. Erbil, J. D. Budai, M. F. Chisholm, L. A. Boather, and B. J. Wilkens, Phys. Rev. B **49**, 14 865 (1994).

[7] J. S. Speck, A. Seifert, W. Pompe, and R. Ramesh, J. Appl. Phys. **76**, 477 (1994).

[8] S. Stemmer, S. K. Streiffer, F. Ernst, and M. Rühle, Philos. Mag. A **71**, 713 (1995).

[9] A. Seifert, F. F. Lange, and J. S. Speck, J. Mater. Res. **10**, 680 (1995).

[10] Y. M. Kang, J. K. Ku, and S. Baik, J. Appl. Phys. **78**, 2601 (1995).

[11] C. M. Foster, Z. Li, M. Buckett, D. Miller, P. M. Baldo, L. E. Rehn, G. R. Bai, D. Guo, H. You, and K. L. Merkle, J. Appl. Phys. **78**, 2607 (1995).

[12] W.-Y. Hsu and R. Raj, Appl. Phys. Lett. **67**, 792 (1995).

[13] S. Kim, S. Hishita, Y. M. Kang, and S. Baik, J. Appl. Phys. **78**, 5604 (1995).

[14] C. M. Foster, W. Pompe, A. C. Daykin, and J. S. Speck, J. Appl. Phys. **79**, 1405 (1996).

[15] M. J. Nystrom, B. W. Wessels, J. Chen, and T. J. Marks, Appl. Phys. Lett. **68**, 761 (1996).

[16] V. Gopalan and R. Raj, Appl. Phys. Lett. **68**, 1323 (1996).

[17] K. S. Lee and S. Baik, J. Appl. Phys. **85**, 1995 (1999).

[18] S. P. Alpay, V. Nagarajan, L. A. Bendersky, M. D. Vaudin, S. Aggarwal, R. Ramesh, and A. L. Roytburd, J. Appl. Phys. **85**, 3271 (1999).

[19] C. S. Ganpule, V. Nagarajan, H. Li, A. S. Ogale, D. E. Steinhauer, S. Aggarwal, E. Williams, and R. Ramesh, Appl. Phys. Lett. **77**, 292 (2000).

[20] J. Lettieri, Y. Jia, M. Urbanik, C. I. Weber, J-P. Maria, D. G. Schlom, H. Li, R. Ramesh, R. Uecker, and P. Reiche, Appl. Phys. Lett. **73**, 2923 (1998).

[21] A. L. Roytburd, in *Heteroepitaxy of Dissimilar Materials*, edited by R. F. C. Ferrow, J. P. Harbison, P. S. Peercy, and A. Zangwill, Mater. Res. Soc. Symp. Proc. No. 221 (Material Research Society, Pittsburgh, 1991), p. 225.

[22] A. L. Roytburd and Y. Yu, Ferroelectrics **144**, 137 (1993).

[23] W. Pompe, X. Gong, Z. Suo, and J. S. Speck, J. Appl. Phys. **74**, 6012 (1993).

[24] J. S. Speck and W. Pompe, J. Appl. Phys. **76**, 466 (1994).

[25] J. S. Speck, A. C. Daykin, A. Seifert, A. E. Romanov, and W. Pompe, J. Appl. Phys. **78**, 1696 (1995).

[26] N. A. Pertsev and A. G. Zembilgotov, J. Appl. Phys. **78**, 6170 (1995); **80**, 6401 (1996).

[27] N. A. Pertsev, G. Arlt, and A. G. Zembilgotov, Microelectron. Eng. **29**, 135 (1995).

[28] N. A. Pertsev, G. Arlt, and A. G. Zembilgotov, Phys. Rev. Lett. **76**, 1364 (1996).

[29] A. E. Romanov, W. Pompe, and J. S. Speck, J. Appl. Phys. **79**, 4037 (1996).

[30] N. A. Pertsev and A. Yu. Emelyanov, Phys. Solid State **39**, 109 (1997).

[31] N. A. Pertsev and A. Yu. Emelyanov, Appl. Phys. Lett. **71**, 3646 (1997).

[32] A. L. Roytburd, J. Appl. Phys. **83**, 228 (1998); **83**, 239 (1998).

[33] S. P. Alpay and A. L. Roytburd, J. Appl. Phys. **83**, 4714 (1998).

[34] A. E. Romanov, M. J. Lefevre, J. S. Speck, W. Pompe, S. K. Streiffer, and C. M. Foster, J. Appl. Phys. **83**, 2754 (1998).

[35] A. E. Romanov, A. Vojta, W. Pompe, M. J. Lefevre, and J. S. Speck, Phys. Status Solidi A **172**, 225 (1999).

[36] N. A. Pertsev and V. G. Koukhar, Phys. Rev. Lett. **84**, 3722 (2000).

[37] A. Yu. Emelyanov, N. A. Pertsev, and E. K. H. Salje, J. Appl. Phys. **89**, 1355 (2001).

[38] N. A. Pertsev, A. G. Zembilgotov, and A. K. Tagantsev, Phys. Rev. Lett. **80**, 1988 (1998); Ferroelectrics **223**, 79 (1999).

[39] N. A. Pertsev, A. G. Zembilgotov, S. Hoffmann, R. Waser, and A. K. Tagantsev, J. Appl. Phys. **85**, 1698 (1999).

[40] F. Jona and G. Shirane, *Ferroelectric Crystals* (MacMillan, New York, 1962).

[41] A. J. Bell and L. E. Cross, Ferroelectrics **59**, 197 (1984).

[42] M. J. Haun, E. Furman, S. J. Jang, H. A. McKinstry, and L. E. Cross, J. Appl. Phys. **62**, 3331 (1987).

[43] O. Auciello, J. F. Scott, and R. Ramesh, Phys. Today **51**, (7), 22 (1998).

[44] N. Setter and R. Waser, Acta Mater. **48**, 151 (2000).

[45] L. D. Landau, E. M. Lifshitz, and L. P. Pitaevskii, *Electrodynamics of Continuous Media* (Pergamon, Oxford, 1984).

[46] A. K. Tagantsev, Cz. Pawlaczyk, K. Brooks, M. Landivar, E. Colla, and N. Setter, Integr. Ferroelectr. **6**, 309 (1995).

[47] Y. Watanabe, Phys. Rev. B **57**, 789 (1998).

[48] E. A. N. Love, *A Treatise on the Mathematical Theory of Elasticity* (Dover, New York, 1944).

[49] J. P. Hirth and J. Lothe, *Theory of Dislocations* (McGraw-Hill, New York, 1968).

[50] The list of material parameters (in SI units, temperature T in °C) used in the calculations. For PT: $\alpha_1 = 3.8(T - 479) \times 10^5$, $\alpha_{11} = -7.3 \times 10^7$, $\alpha_{12} = 7.5 \times 10^8$, $\alpha_{111} = 2.6 \times 10^8$, $\alpha_{112} = 6.1 \times 10^8$, $\alpha_{123} = -3.7 \times 10^9$, $Q_{11} = 0.089$, $Q_{12} = -0.026$, $Q_{44} = 0.0675$, $s_{11} = 8.0 \times 10^{-12}$, $s_{12} = -2.5 \times 10^{-12}$, $s_{44} = 9.0 \times 10^{-12}$. For BT: $\alpha_1 = 3.34(T - 108) \times 10^5$, $\alpha_{11} = 4.69(T - 120) \times 10^6 - 2.02 \times 10^8$, $\alpha_{12} = 3.23 \times 10^8$, $\alpha_{111} = -5.52(T - 120) \times 10^7 + 2.76 \times 10^9$, $\alpha_{112} = 4.47 \times 10^9$, $\alpha_{123} = 4.91 \times 10^9$, $Q_{11} = 0.11$, $Q_{12} = -0.043$, $Q_{44} = 0.059$, $s_{11} = 8.3 \times 10^{-12}$, $s_{12} = -2.7 \times 10^{-12}$, $s_{44} = 9.24 \times 10^{-12}$.

[51] Numerical calculations confirm that, within the stability range R_d of the $c/a/c/a$ state in the S_m-T plane, the rotation of domain walls away from the assumed orientation parallel to the {101} crystallographic planes of the prototypic cubic phase is energetically unfavorable.

[52] $\alpha_{11}^* = \alpha_{11} + [(Q_{11}^2 + Q_{12}^2)s_{11} - 2Q_{11}Q_{12}s_{12}]/[2(s_{11}^2 - s_{12}^2)]$, $\alpha_{12}^* = \alpha_{12} - [(Q_{11}^2 + Q_{12}^2)s_{12} - 2Q_{11}Q_{12}s_{11}]/(s_{11}^2 - s_{12}^2) + Q_{44}^2/(2s_{44})$.

[53] Y. S. Touloukian, R. K. Kirby, R. E. Taylor, and T. Y. R. Lee, *Thermal Expansion, Nonmetallic Solids*, Thermophysical Properties of Matter, Vol. 13 (Plenum, New York, 1997).

[54] D. H. Chen, K. R. Udayakumar, C. J. Gaskey, and L. E. Cross, Appl. Phys. Lett. **67**, 3411 (1995).